# Fermionic spinon theory of the

# hourglass spin excitation spectrum of the cuprates

Alexander Nikolaenko\* Pietro M. Bonetti Subir Sachdev

Alexander Nikolaenko, Pietro M. Bonetti, Subir Sachdev

Department of Physics, Harvard University, Cambridge MA 02138, USA

Email Address: onikolaienko@g.harvard.edu

Subir Sachdev

Center for Computational Quantum Physics, Flatiron Institute, 162 5th Avenue, New York, NY 10010, USA

We present a theory for the spin fluctuation spectrum of the hole-doped cuprates in a ground state with period 4 unidirectional charge density wave ('stripe') order. Motivated by recent experimental evidence for a fractionalized Fermi liquid (FL\*) description the intermediate temperature pseudogap metal, we employ a theory of fermionic spinors which are confined with the onset of stripe. charge density wave ('stripe') order. Motivated by recent experimental evidence for a fractionalized Fermi liquid (FL\*) description of the intermediate temperature pseudogap metal, we employ a theory of fermionic spinons which are confined with the onset of stripe order at low temperatures. The theory produces the 'hourglass' spectrum near stripe-ordering wavevector observed by neutron scattering. Additional scattering from spinon continua and bound states appears at higher energies and elsewhere in the Brillouin zone,

tering. Additional scattering from spinon continua and bound states appears at higher energies and elsewhere in the Brillouin zone, and could be observed by neutron or X-ray scattering.

1 Introduction

There have been a number of earlier studies suggesting the relevance of fractionalized spinon excitations (which carry spin 1/2 and electrical charge 0) to square lattice antiferromagnets [1, 2, 3, 4, 5, 6]. Recent work [7, 8, 9, 10, 11], reviewed in Ref. [12], has argued that such spinons are the key to understanding a number of observations in the underdoped cuprates. These arguments rely on the fractionalized Fermi liquid (FL\*) theory [13, 14, 15, 16, 17, 18, 19, 20, 21, 22] of the pseudogap phase: the FL\* state of the doped square lattice antiferromagnet [23, 24, 25, 26, 27, 7] has 4 Fermi pockets of spin-1/2 charge e quasiparticles, each of fractional area p/8, so that the total density of mobile quasiparticles is p. Such a state does not obey the Luttinger Fermi surface area [28], but does satisfy the Oshikawa anomaly [29] by the presence of additional spinon excitations [13, 15, 16, 18, 21].

Compelling evidence for such a FL\* state comes from recent angle-dependent magnetoresistance (ADMR) measurements [30, 31]. The ADMR displays significant evidence for the presence of hole pockets, and the Yamaji effect is consistent with the FL\* pocket area of p/8 [32]. Moreover, the Yamaji effect requires coherent inter-layer electronic transport, which is present for FL\*, and unlikely for other pseudogap candidates [32]. Other recent arguments for the FL\* description of the pseudogap are summarized in Section 4.

In this paper, we turn to the role of spinons in the spin-fluctuation spectrum, where they have a direct role. Our focus is on the well-studied 'hourglass' spectrum of the stripe state observed by neutron scattering in the cuprates near hole doping p = 1/8 [33, 34, 35].

tering in the cuprates near hole doping p = 1/8 [33, 34, 35].

We use the  $\pi$ -flux spin liquid theory for the underlying square lattice antiferromagnet [36, 37, 38]. This has fermionic spinon excitations which carry spin S=1/2 and a dispersion with 2 massless Dirac nodes in the square lattice Brilloin zone. The spinons are coupled to an emergent SU(2) gauge field (the gauge SU(2) is distinct from, and commutes with, the spin rotation SU(2)). Fluctuations of the SU(2) gauge field in the insulator are expected to lead to confinement of the spinons into either the Néel state or the valence bond solid (VBS) state, but there is evidence for a deconfined critical state of the spinons between the Néel and VBS states [39, 40, 41]. The free spinon dynamic structure factor is reviewed in Section 2.1, and this is in good correspondence with numerical studies of the Néel-VBS transition [3]. The free spinon theory exhibits significant low energy spectral weight near momenta  $(\pi, \pi)$ ,  $(\pi, 0)$ , and (0, 0); Ref. [10] argued that SU(2) gauge fluctuations strongly suppress the spectral weight near momenta (0,0) and  $(\pi,0)$ .

Resonant inelastic X-ray scattering (RIXS) experiments have investigated the high energy spin fluctuation spectrum in the cuprates [42, 43, 44]. Ref. [45] has noted that the broad continuum scattering between momenta (0,0) and  $(\pi,0)$  bear a strong resemblance to the continuum spectral weight in the frustrated square lattice antiferromagnet near the Néel-VBS transition [3]. The energy scales match well, and the main difference is that the insulating antiferromagnet has gapless spectral weight at  $(\pi,0)$ , while the doped cuprate has little spectral weight below  $\sim 200$  meV. This difference could be a consequence of the doped carriers, whose influence will be studied here.

The present paper will study a different route to confinement of the spinons at low energies, appropriate to the doped cuprates [8]. We will assume a charge density wave (CDW) with static long-range order which is produced by the condensation of a Higgs field B [10]. This Higgs field carries a fundamental SU(2) gauge charge, and so its condensation gaps out all components of the SU(2) gauge field. The resulting B-condensed phase is 'topologically trivial', but nevertheless, signatures of the deconfined spinons can emerge at higher energies. And at low energies, as we shall demonstrate, such a spinon theory is able to reproduce the 'hourglass' spectrum of the CDW ('stripe') state. Our approach differs from other theories of the hourglass [46, 47, 48, 49] by using spin S = 1/2 excitations in a background of charge order, whereas the earlier works considered spin S = 1 paramagnon excitations.

We study the spin susceptibility of the underdoped cuprates using the Ancilla Layer Model (ALM) studied extensively in previous works [27, 50, 51, 9, 10, 12]. The ALM offers a unified description of both the FL\* pseudogap metal with small Fermi surface, and a conventional Fermi liquid with large Fermi surface. It also hosts fractionalized spinon excitations that ensure consistency with the Oshikawa anomaly. In the following sections, we examine how these excitations affect the spin structure factor and make predictions for future neutron scattering experiments.

In Section 2 we introduce the ALM, and derive the expressions for susceptibility in the presence of CDW order. In Section 3 we present our calculation of the spin structure factor, discuss the role of spinons and compare our calculations to experiments. Finally, we conclude in Section 4 by recalling experimental and theoretical evidence for FL\* in the hole-doped cuprates.

# 2 Theory

We start this section by formulating the ALM. The model has three layers: the first level consists of electrons described by tight-binding model, while the second and the third layers are filled with spins with Heisenberg interaction between them. The Hamiltonian of the ALM is [27, 7, 9]:

$$H = \sum_{i,j,\alpha} \left\{ -t_{ij} c_{i,\alpha}^{\dagger} c_{j,\alpha} + J_K \mathbf{S}_{c,i} \cdot \mathbf{S}_{1,i} + J_1 \mathbf{S}_{1,i} \cdot \mathbf{S}_{1,j} + J_{\perp} \mathbf{S}_{1,i} \cdot \mathbf{S}_{2,i} + J_2 \mathbf{S}_{2,i} \cdot \mathbf{S}_{2,j} \right\},$$
(1)

where  $i, j \in \Lambda$ , with  $\Lambda = \{(x, y) | x, y \in \mathbb{Z}\}$  being a two-dimensional square lattice. For the first layer we employ the tight-binding parameters t = 0.22 (nearest neighbor hopping), t' = -0.034 (second neighbor hopping), t'' = 0.036 (third neighbor hopping), t''' = -0.007 (fourth neighbor hopping), and a chemical potential  $\mu_c = -0.24$  (all in units of eV). These values have been extracted by fitting photoemission data from Ref. [52] in the overdoped regime, where large Fermi surface is clearly visible.

We use the Schwinger-fermion representation for the second (a = 1) and third (a = 2) layer spins:  $S_{a,i} = f^{\dagger}_{a,i,\alpha} \sigma_{\alpha\beta} f_{a,i,\beta}$  with the imposed constraint  $\sum_{\alpha} f^{\dagger}_{a,i,\alpha} f_{a,i,\alpha} = 1$ , satisfied at every lattice site i. Throughout the paper, we adopt a mean-field approach and neglect all gauge field fluctuations emerging from the redundancy of the parton construction. Within the mean-field theory, the interacting terms in the Hamiltonian simplify to:

$$H_{f_1,f_1} + H_{c,f_1} + H_{f_1,f_2} = t_{1,ij} f_{1,i,\alpha}^{\dagger} f_{1,j,\alpha} + \Phi(f_{1,i,\alpha}^{\dagger} c_{i,\alpha} + c_{i,\alpha}^{\dagger} f_{1,i,\alpha}) + \left[ i B_{1,i} f_{2,i,\alpha}^{\dagger} f_{1,i,\alpha} + i B_{2,i} f_{2,i,\alpha} \varepsilon_{\alpha\beta} f_{1,i,\beta} + \text{h.c.} \right],$$
(2)

where  $\Phi \propto J_K \langle f_{1,\mathbf{i},\alpha}^{\dagger} c_{\mathbf{i},\alpha} \rangle \in \mathbb{R}$  and  $B_{1,\mathbf{i}} \propto J_{\perp} \langle f_{1,\mathbf{i},\alpha}^{\dagger} f_{2,\mathbf{i},\alpha} \rangle$ ,  $B_{2,\mathbf{i}} \propto J_{\perp} \langle f_{1,\mathbf{i},\alpha}^{\dagger} \varepsilon_{\alpha\beta} f_{2,\mathbf{i},\beta}^{\dagger} \rangle$ , with  $\varepsilon_{\alpha\beta}$  the unit antisymmetric tensor. The second layer is characterized by the hopping parameters  $t_1 = 0.1, t_1' = -0.03, t_1'' = 0.00$ 

-0.01, a chemical potential  $\mu_f = 0.009$ , and a hybridization with the first layer  $\Phi = 0.09$ . The finite hybridization between the first and second layers leads to the emergence of four Fermi pockets in the Brillouin zone with area p/8. Moreover, the intensity at back side of the pockets is subdued, which is consistent with Fermi arcs features observed in photoemission experiments. The parameters were chosen to reproduce the photoemission data for Bi2201 at a doping level of p = 0.206 [7, 52]. The B field would be discussed later, to incorporate the effects of CDW order. For now we assume  $B_{a,i} = 0$ .

A nonzero value of  $\Phi$  reconstructs the top layer large Fermi surface, of (hole) volume 1+p, into four hole pockets of total volume p. Because no translation symmetry breaking is occurring at this point, this is at odds with the conventional formulation of Luttinger's theorem. To account for its violation, we assume the presence of a quantum spin liquid in the bottom layer, hosting fractionalized spinon excitations that account for the missing Luttinger volume [29, 13, 15]. In particular, we choose a  $\pi$ -flux spin liquid Ansatz of the form:

$$H_{f_2,f_2} = it^{f_2} f_{2,\mathbf{i},\alpha}^{\dagger} e_{\mathbf{i},\mathbf{j}} f_{2,\mathbf{j},\alpha} , \qquad (3)$$

with  $e_{i,j} = -e_{j,i}$  and in the chosen gauge  $e_{i,i+\hat{x}} = 1$ ,  $e_{i,i+\hat{y}} = (-1)^x$ . We also set  $t^{f_2} = 0.14\,eV$  similar to Ref. [9]. The chosen gauge is not manifestly translation invariant in the x-direction. In fact, translations along the x-axis are implemented projectively  $f_{2,i,\alpha} \to (-1)^y f_{2,i,\alpha}$ , implying that all gauge invariant quantities computed with Hamiltonian (3) will be translation invariant. The Hamiltonian  $H_{f_2,f_2}$  can be diagonalized in the momentum space. We consider a supercell with two sites  $\{\delta_i = 0, 1\}$  in the x-direction. After Fourier transform  $f_{2,\delta_i}(\mathbf{r}) = e^{i\mathbf{k}\mathbf{r}} f_{2,\delta_i}(\mathbf{k})$  the Hamiltonian in the basis  $\{f_{2,\delta_i}^{\dagger}(\mathbf{k})\}$  is  $2 \times 2$  matrix with with spectrum  $E_{\pm}(k) = \pm 2t^{f_2} \sqrt{\sin(k_x)^2 + \sin(k_y)^2}$  and  $\mathbf{k}$  is defined in the reduced Brillouin zone BZ' =  $\{(k_x, k_y) \mid k_x \in (-\pi/2, \pi/2), k_y \in (-\pi, \pi)\}$ . The spectrum features two Dirac cones (per spin projection  $\alpha$ ) at  $(k_x, k_y) = (0, 0)$  and  $(k_x, k_y) = (0, \pi)$ .

### 2.1 Bare spin susceptibilities for the $\pi$ -flux spin liquid

The bare  $\pi$ -flux spin-z susceptibility in real space is given by the product of two Green functions:

$$\chi_{\mathbf{i},\mathbf{j}}^{0}(i\Omega_{n}) = \sum_{m=-\infty}^{+\infty} G_{\mathbf{i},\mathbf{j}}(i\omega_{m})G_{\mathbf{j},\mathbf{i}}(i\omega_{m} + i\Omega_{n}), \qquad (4)$$

with  $\omega_m$  and  $\Omega_n$  fermionic and bosonic Matsubara frequencies, respectively, and  $G_{i,j}(i\omega_n) = [i\omega_n - it^{f_2}e_{i,j}]^{-1}$ . As previously discussed, being  $\chi_{i,j}^0(i\Omega_n)$  a gauge invariant object, we expect it to be translation invariant, that is,  $\chi_{i,j}(i\Omega_n) = \chi_{i-j}(i\Omega_n)$ . We define  $\pi$ -flux susceptibility in the momentum basis as

$$\chi^{0}(\omega, \mathbf{q}) = \sum_{i,j} \chi^{0}_{i,j}(i\Omega_{n} \to \omega + i0^{+})e^{-i\mathbf{q}\cdot(i-j)}.$$
 (5)

After analytically continuing to real frequencies and going to momentum basis, we obtain:

$$\chi^{0}(\omega, \boldsymbol{q}) = \sum_{\ell, \ell' = \pm} \sum_{\boldsymbol{k}} \frac{n_{F}(E_{\ell}(\boldsymbol{k})) - n_{F}(E_{\ell'}(\boldsymbol{k} + \boldsymbol{q}))}{\omega + i0^{+} + E_{\ell}(\boldsymbol{k}) - E_{\ell'}(\boldsymbol{k} + \boldsymbol{q})} |\langle E_{\ell'}(\boldsymbol{k} + \boldsymbol{q}) | E_{\ell}(\boldsymbol{k}) \rangle|^{2},$$
(6)

with  $E_{\alpha}(\mathbf{k})$  and  $|E_{\alpha}(\mathbf{k})\rangle$  denoting an eigenvalues and eigenvectors of the Hamiltonian in Eq. (3),  $\sum_{\mathbf{k}}$  is a shorthand for  $\int_{\mathbf{k}\in\mathrm{BZ'}}\frac{d^2\mathbf{k}}{(2\pi)^2}$ , and  $n_F(x)$  is the Fermi function.

#### 2.2 Bare susceptibilities in the presence of charge density wave order

We now consider the susceptibilities when  $B_{a,i} \neq 0$ . As found in Ref. [8], the condensation of the field  $B_{a,i}$  has both effects of fully Higgsing the SU(2) gauge group associated with the Schwinger fermion decomposition in the bottom layer, and breaking some physical global symmetries, such as translations,

time reversal, or U(1) charge conservation, depending on the spatial pattern of  $B_{a,i}$ . In the following, we choose an Ansatz for  $B_{a,i}$  that only breaks translation symmetry along the x-axis:

$$B_{1,i} = 2b i^{x+y} [\cos \theta + (-1)^x \sin \theta] \cos \left(\frac{K_x x + \phi}{2}\right), \quad B_{2,i} = 0,$$
 (7)

with  $b \in \mathbb{R}$  denoting the amplitude of the wave and  $\phi$  a phase shift. According to [8], the CDW order parameter is given by:

$$\rho_i = B_i^{\dagger} B_i = 2b^2 [1 + (-1)^x \sin 2\theta] [\cos (K_x x + \phi) + 1]. \tag{8}$$

One can check that the above Ansatz gives vanishing current and superconducting order parameters,  $\Re[B_{i}^{\dagger}e_{i,j}B_{j}]=0$ ,  $B_{a,i}\varepsilon_{ab}e_{i,j}B_{b,j}=0$ . In the following, we restrict ourselves to a period-4 bond-centered CDW, given by  $K_{x}=\frac{\pi}{2}, \ \phi=\frac{\pi}{4}$ .

We consider two different effects of the  $B_{a,i}$  condensate on the fermionic degrees of freedom: one is given the last terms in Eq. (2), which couple the bottom layer spinons to the top two layers, making them indistinguishable from physical electrons; a second effect is that it could modify the  $\pi$ -flux Ansatz into

$$H_{f_2,f_2} = it^{f_2} (1 + \lambda Q_{i,j}) f_{2,i,\alpha}^{\dagger} e_{i,j} f_{2,j,\alpha}, \tag{9}$$

with

$$Q_{i,i+\hat{x}} = \Im[B_i^{\dagger} e_{i,i+\hat{x}} B_{i+\hat{x}}] = 2b^2 \cos 2\theta \left[\cos(K_x(x+1/2) + \phi) + \cos(K_x/2)\right],$$

$$Q_{i,i+\hat{y}} = \Im[B_i^{\dagger} e_{i,i+\hat{y}} B_{i+\hat{y}}] = 2b^2 [(-1)^x + \sin 2\theta] [\cos(K_x x + \phi) + 1].$$
(10)

Note that this last term cannot be derived with the sole use of mean-field theory, but it can be thought of as emerging upon integrating out of some high-energy degrees of freedom. Similarly to the previous case, we introduce a unit cell consisting of four sites  $\delta_i = 0, 1, 2, 3$  with basis  $\{f_{2,\delta_i}^{\dagger}(\mathbf{k})\}$  and the following Fourier transform between real and Fourier space:  $f_{2,\delta_i}(\mathbf{r}) = e^{i\mathbf{k}\mathbf{r}} f_{2,\delta_i}(\mathbf{k})$  The Hamiltonian in Eq. (9) becomes a  $4 \times 4$  matrix. On site constraint  $\langle f_{2,i}^{\dagger} f_{2,i} \rangle = 1$  is also satisfied since the Hamiltonian remains particle-hole symmetric. Eq. (4) is readily generalized in the new basis:

$$\chi_{i,j}^{0}(iq_n) = \sum_{\omega_n,k,q} G_{\delta_i\delta_j}(i\omega_n + iq_n, \mathbf{k} + \mathbf{q})G_{\delta_j,\delta_i}(i\omega_n, \mathbf{k})e^{i\mathbf{q}(i-j)} = \chi_{\delta_i\delta_j}^{0}(iq_n, \mathbf{q})e^{i\mathbf{q}(i-j)}.$$
 (11)

After analytically continuing to real frequencies, we obtain:

$$\chi_{\delta_{i},\delta_{j}}^{0}(\omega,\boldsymbol{q}) = \sum_{\alpha,\beta=1,\dots,4} \sum_{\boldsymbol{k}} \frac{n_{F}(E_{\alpha}(\boldsymbol{k})) - n_{F}(E_{\beta}(\boldsymbol{k}+\boldsymbol{q}))}{\omega + i\delta + E_{\alpha}(\boldsymbol{k}) - E_{\beta}(\boldsymbol{k}+\boldsymbol{q})} F_{\delta_{i}}^{\alpha}(\boldsymbol{k}) F_{\delta_{j}}^{\alpha}(\boldsymbol{k})^{*} F_{\delta_{j}}^{\beta}(\boldsymbol{k}+\boldsymbol{q}) F_{\delta_{i}}^{\beta}(\boldsymbol{k}+\boldsymbol{q})^{*},$$
(12)

with the form factors  $F_{f_2,\delta_i}^{\alpha}(\mathbf{k}) = \langle f_2, \delta_i | | E_{\alpha}(\mathbf{k}) \rangle$  and  $| E_{\alpha}(\mathbf{k}) \rangle$  being eigenvectors of the Hamiltonian in Eq. (9).

Now, the interacting part of the Hamiltonian is:

$$H_{int} = \sum_{ij} J_{ij} (1 + gQ_{ij}^b) f_{i\alpha}^{\dagger} f_{j\alpha} f_{j\beta}^{\dagger} f_{i\beta} = \sum_{ij} \tilde{J}_{ij} f_{i\alpha}^{\dagger} f_{j\alpha} f_{j\beta}^{\dagger} f_{i\beta}, \tag{13}$$

where  $J_{ij}$  is a Heisenberg coupling. We will include RPA corrections from this interaction, following the application of such methods to the triangular lattice antiferromagnet [53, 54, 55]. After using the Fourier representation with  $J_{ij} = \sum_q J_{\delta_i \delta_j}(\mathbf{q}) e^{i\mathbf{q}(i-j)}$  and summing up the series, the RPA result in the spin-spin channel in matrix notation reads:

$$\chi^{RPA}(\omega, \mathbf{q}) = \chi^0(\omega, \mathbf{q})(1 - \tilde{J}(\mathbf{q})\chi^0(\omega, \mathbf{q}))^{-1}.$$
(14)

Although  $\chi^{RPA}(\omega, \boldsymbol{q})$  is  $4 \times 4$  matrix, Eq. (5) provides an efficient route to extract an experimentally relevant expression. Noting that  $\chi^{RPA}_{\delta_i,\delta_j}(\omega, \boldsymbol{q} + nK_x)e^{inK_x(\delta_i - \delta_j)} = \chi^{RPA}_{\delta_i,\delta_j}(\omega, \boldsymbol{q})$  and accounting for charge density wave (CDW) order along both spatial directions, the experimentally observable susceptibility can be

written as:  $\chi^{exp}(\omega, \mathbf{q}) = \sum_{\delta_i, \delta_j} \left( \chi_{\delta_i, \delta_j}^{RPA}(\omega, q_x, q_y) + \chi_{\delta_i, \delta_j}^{RPA}(\omega, q_y, q_x) \right)$ . For the expression of the Hamiltonian, and  $\tilde{J}$  in the matrix notation see Appendix A.

The full Hamiltonian, including couplings to electrons, could be written as:

$$H = \psi_{\mathbf{k}}^* \begin{pmatrix} H_{c,c}(\mathbf{k}) & \Phi^{\dagger} & 0\\ \Phi & H_{f_1,f_1}(\mathbf{k}) & -ig_e B^{\dagger}\\ 0 & ig_e B & H_{f_2,f_2}(\mathbf{k}) \end{pmatrix} \psi_{\mathbf{k}}, \tag{15}$$

where  $\psi_{\mathbf{k}} = (c_{\mathbf{k},\delta_1,\uparrow}, \dots, c_{\mathbf{k},\delta_4,\uparrow}, f_{1,\mathbf{k},\delta_1,\uparrow}, \dots, f_{1,\mathbf{k},\delta_4,\uparrow}, f_{2,\mathbf{k},\delta_1,\uparrow}, \dots, f_{2,\mathbf{k},\delta_4,\uparrow})$  consists of three layers in the extended CDW basis and  $g_e$  determines the strength of hybridization between the third and second layers. The bare susceptibility is determined analogous to Eq. (11):

$$\chi_{\delta_i,\delta_j}^{f_2,f_2}(iq_n, \mathbf{q})^0 = \sum_{\mathbf{k},i\omega_n} G_{\delta_i,\delta_j}^{f_2f_2}(iq_n + i\omega_n, \mathbf{k} + \mathbf{q}) G_{\delta_j,\delta_i}^{f_2f_2}(i\omega_n, \mathbf{k})$$
(16)

And after performing Matsubara summation and analytically continuing to real frequencies:

$$\chi_{\delta_{i},\delta_{j}}^{f_{2}f_{2}}(\omega,\boldsymbol{q})^{0} = \sum_{\alpha,\beta=1,\dots,12} \sum_{\boldsymbol{k}} \frac{n_{F}(E_{\alpha}(\boldsymbol{k})) - n_{F}(E_{\beta}(\boldsymbol{k}+\boldsymbol{q}))}{\omega + i\delta + E_{\alpha}(\boldsymbol{k}) - E_{\beta}(\boldsymbol{k}+\boldsymbol{q})} F_{f_{2},\delta_{i}}^{\alpha}(\boldsymbol{k}) F_{f_{2},\delta_{j}}^{\alpha}(\boldsymbol{k})^{*} F_{f_{2},\delta_{j}}^{\beta}(\boldsymbol{k}+\boldsymbol{q}) F_{f_{2},\delta_{i}}^{\beta}(\boldsymbol{k}+\boldsymbol{q})^{*}, \quad (17)$$

with the form factors  $F_{f_2,\delta_i}^{\alpha}(\mathbf{k}) = \langle f_2, \delta_i | | E_{\alpha}(\mathbf{k}) \rangle$  and  $| E_{\alpha}(\mathbf{k}) \rangle$  being eigenvectors of the Hamiltonian in Eq. (15). Eqs. (14,17) provide the most general expressions for the susceptebility and we use them in the next section to analyze the spin structure factor near optimal doping.

### 3 Discussion

In this section, we analyze the spin-structure factor obtained from our model and compare it with experimental observations in various cuprate compounds. We assume that the dominant contribution to the spin-structure factor comes from the third layer which is a  $\pi$ -flux spin liquid described by the Hamiltonian in Eq. (3). The system is treated within the mean-field approximation, neglecting the SU(2) fluctuations of the gauge field. Fig. 1 shows the imaginary part of the spin susceptibility for the third layer. A similar calculation was previously done in Ref. [4]. As shown, there is a gapless spinon continuum centered at  $(\pi, \pi)$  in momentum space, exhibiting a Dirac-like dispersion.

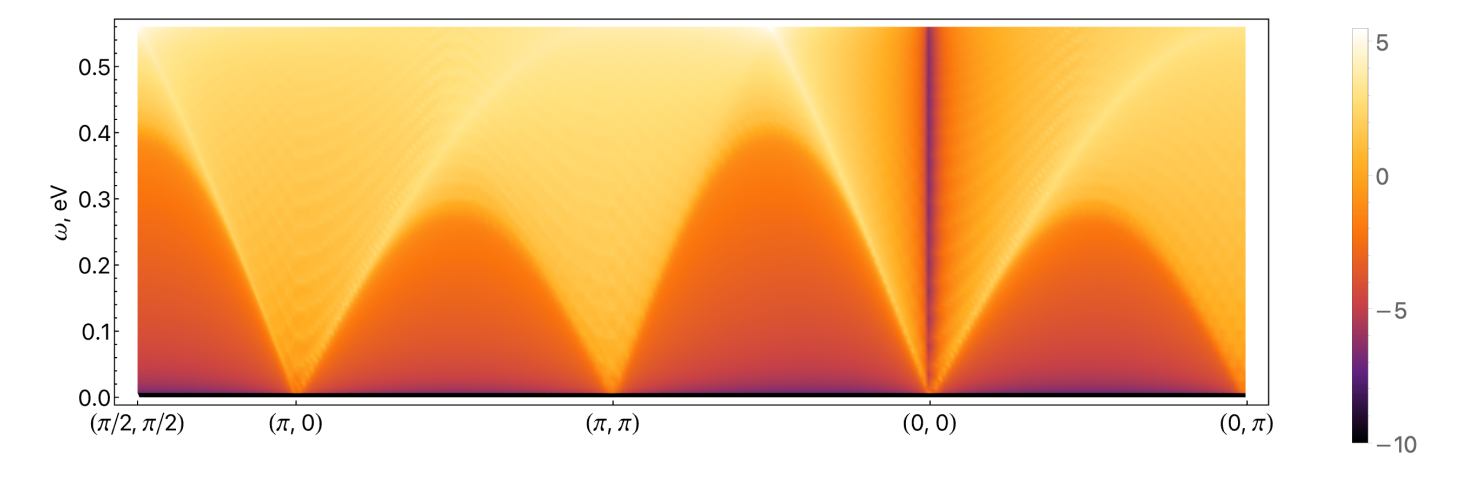


Figure 1: Bare  $\pi$ -flux spin structure factor  $-\Im\chi^0(\omega,q)$  on a logarithmic scale along high-symmetry directions in the Brillouin zone. The regions of strong intensity correspond to a spinon continuum, having a Dirac-like shape near  $(\pi,\pi)$ .

As discussed in the previous section, the condensation of the B-field Higgs the SU(2) gauge field and leads to CDW order. We assume that the CDW order is bond-centered and has a period of four unit

cells. The CDW potential opens a gap in the  $\pi$ -flux Dirac-like spectrum and moves a spinon continuum to higher energies. This gap directly manifests in the spin-structure factor, as illustrated in Fig. 2. The spectral intensity also varies in a complex way inside the spinon continuum, reflecting scattering between different bands. Throughout this work, we use b=1.3,  $\lambda=1$ , and  $\theta=0.45$  to measure the amplitude and phase of the CDW order.

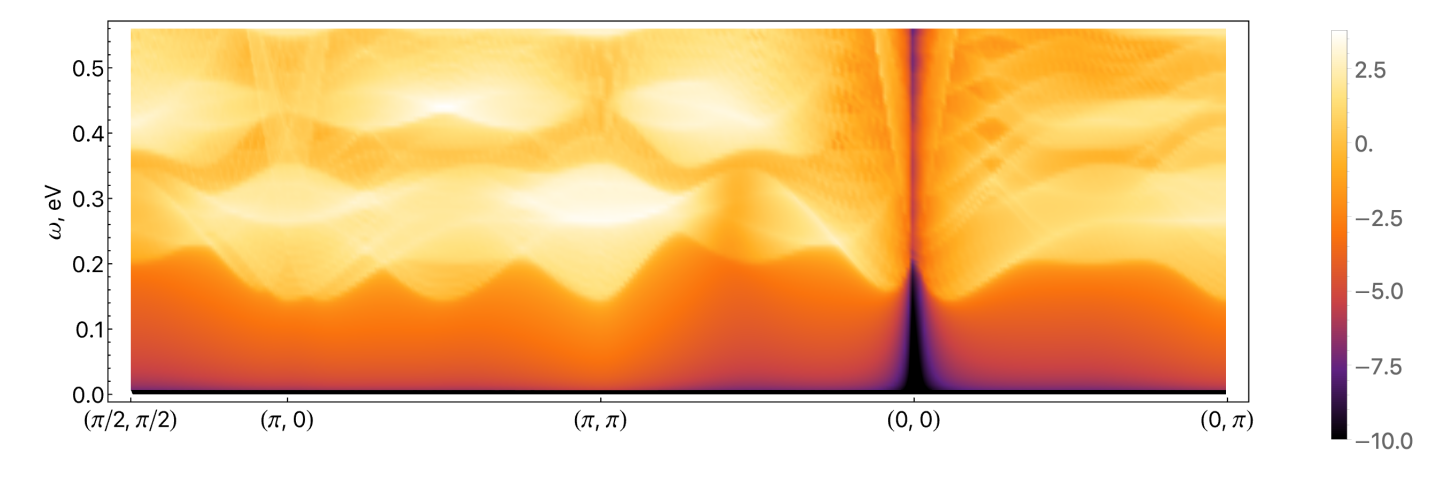


Figure 2: Bare  $\pi$ -flux spin structure factor  $-\Im\chi^0(\omega,q)$  on a logarithmic scale in the presence of CDW order, averaged over the x and y-directions. As a result of CDW order, the gap opens throughout the Brillouin zone, moving the spinon continuum to higher energies.

We examine the effect of the interacting part of the Hamiltonian using the results of the previous section, see Eq. (13). Incorporating interactions within the RPA framework leads to a renormalized spin susceptibility given by Eq. (14). Fig. 3 demonstrates that the including interactions leads to an emergent collective excitation (a triplon branch) below the spinon continuum. We choose Heisenberg couplings J = 0.235, J' = -0.3J, J'' = 0.6J, J''' = 0.02J, J'''' = 0.45J to achieve the dispersion that reproduces the characteristic hourglass-shaped spectrum. This type of spectrum has been observed in numerous neutron-scattering experiments on cuprate materials [33, 34, 35].

Although the model contains several phenomenological parameters, we note that the hourglass-shaped spectrum can be reproduced using only the J, J', and J'' couplings. However, in that case, the characteristic features appear at lower energies and are less distinct. The CDW order affects the Heisenberg couplings as well, see Eq. (13), and we chose g = 0.1 to control the relative amplitude.

Importantly, the hourglass profile arises from averaging the CDW order over both spatial directions. Without this averaging, two distinct triplon branches appear, as illustrated in Fig. 4. Panels (a) and (b) correspond to the CDW order along the x and y directions correspondingly. In panel (a), the triplon branch exhibits a minimum at  $(\pi, \pi)$ , whereas in panel (b) the minimum is shifted away from  $(\pi, \pi)$ . The combination of the two produces the characteristic hourglass-shaped dispersion.

In Appendix B we analyze RPA renormalized spin structure factor without the CDW order. While the triplon branch is observable, it does not have a typical hourglass shape and the spinon continuum spreads all the way to zero energies, making it harder to relate to the experimental observations.

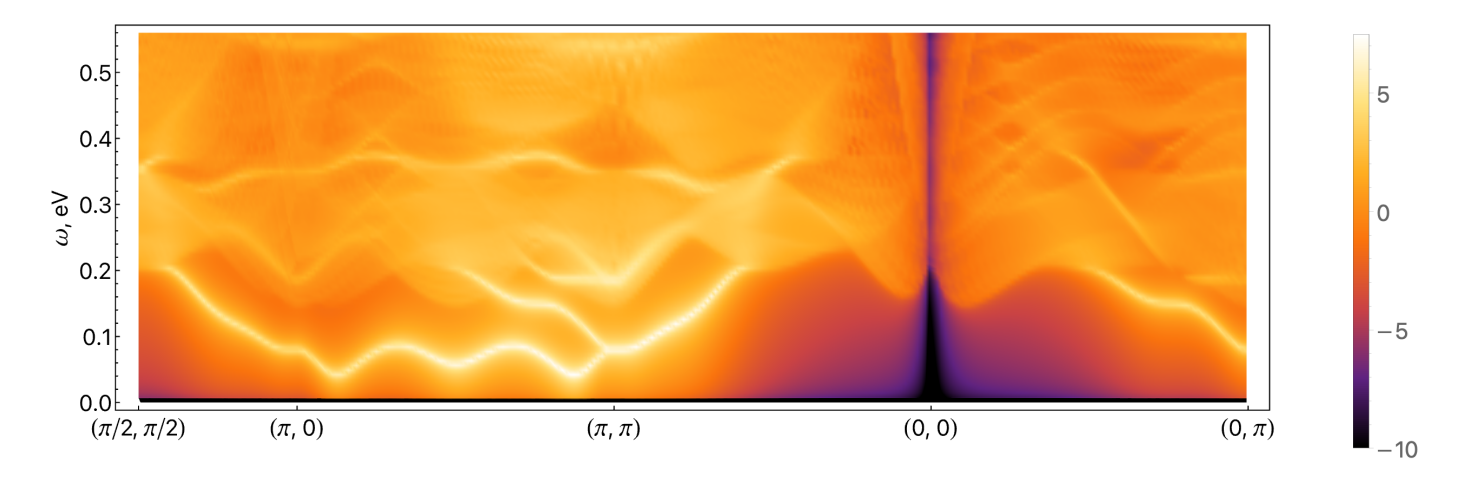


Figure 3: RPA  $\pi$ -flux spin structure factor  $-\Im\chi^{RPA}(\omega,q)$  on a logarithmic scale in the presence of CDW order, averaged over the x and y-directions. RPA corrections to the susceptibility introduce a triplon line-shape of high intensity, having an hourglass-like form near  $(\pi,\pi)$ .

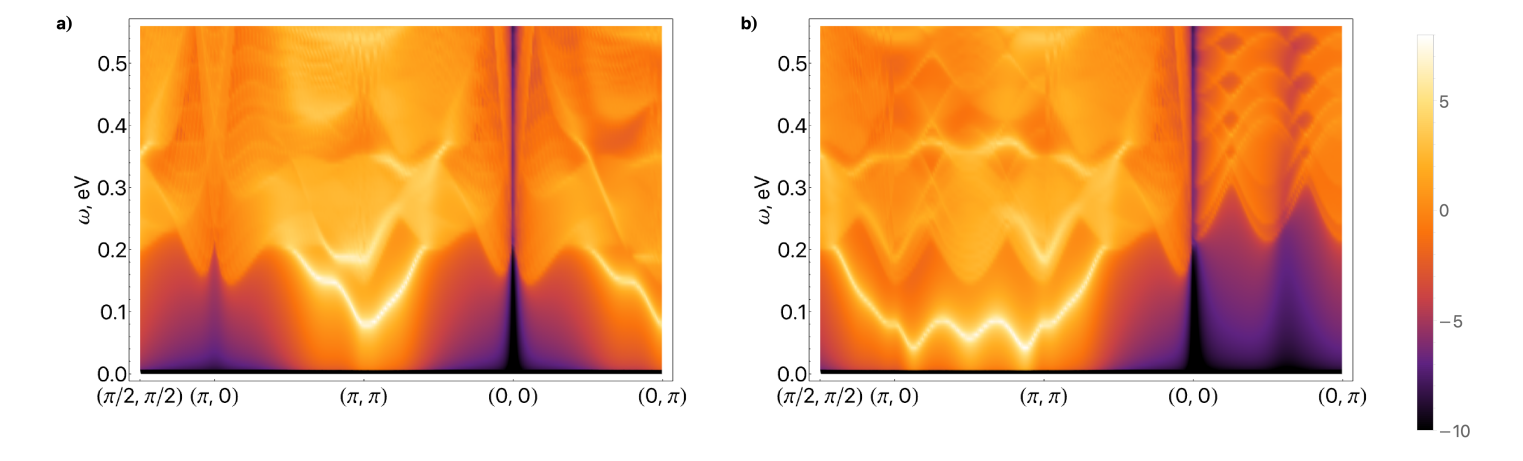


Figure 4: RPA  $\pi$ -flux spin structure factor on a logarithmic scale in the presence of CDW order along the x-direction (a) and along the y direction (b). The minimum of the triplon branch is centered at  $(\pi, \pi)$  when the CDW order is set along the x-direction, and it is shifted from  $(\pi, \pi)$  when the order is along the y-direction, producing a famous hourglass-like spectrum after averaging over both directions.

So far, we have considered only the contribution of the third layer to the spin structure factor, neglecting contributions from the other layers. In principle, however, the full Hamiltonian is given by Eq. (15), and the contribution from the remaining layers is non-negligible. In particular, the first two layers host gapless excitations near the Fermi energy, forming hole pockets, or so-called Fermi arcs. Consequently, their presence is expected to modify the low-energy part of the structure factor, introducing additional spectral weight and damping effects in this regime. Fig. 5 shows that at a finite hybridization strength between the third and second layers ( $g_e = 0.4$ ) the triplon branch and the spinon continuum become noticeably broadened, while the gapped region in the spectrum is softened.

Fig. 6 shows a zoomed-in view of hourglass shaped dispersion when  $q_y$  varies from  $\pi/2$  to  $3\pi/2$ . We observe a clear hourglass shaped triplon excitation, centered around  $(\pi, \pi)$ . The minimum of the hourglass occurs at the incommensurate momenta slightly displaced from  $(\pi, \pi)$ . Notably, in contrast to experimental observations, our calculations show that when the momentum is tuned further away from these minima, the excitation branch rises again. This discrepancy may come from limitations of the theoretical model or from various experimental factors that enhance the magnetic response near  $(\pi, \pi)$ .

We also examine constant-energy cuts across the Brillouin zone, with non-averaged (a)-(d) and averaged (e)-(h) CDW order, see Fig. 7. In particular, panels (a),(b),(e), and (f) demonstrate that below the neck of the hourglass, the intensity maxima are displaced from  $(\pi, \pi)$ . Around  $\omega \approx 80 \, meV$  a pronounced

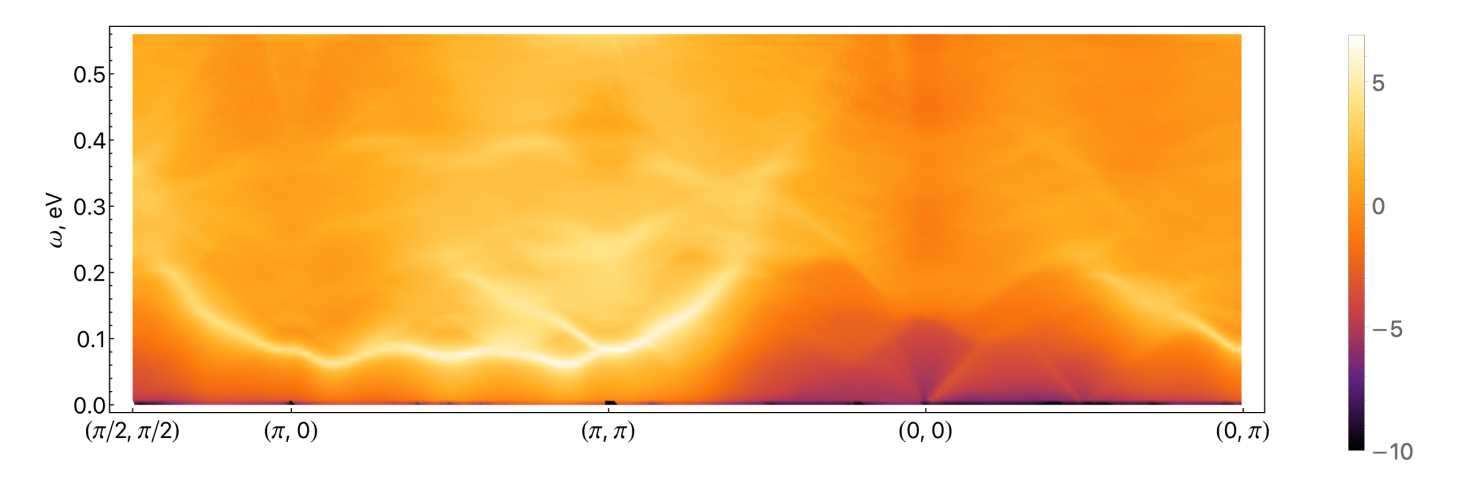


Figure 5: RPA spin structure factor on a logarithmic scale in the presence of CDW order averaged over the x and y-directions, when all three ancilla layers hybridize and contribute to the overall susceptibility. The presence of hole pockets and gapless excitations in the first two layers result in the finite spectral weight inside the CDW gap and broadens the triplon branch.

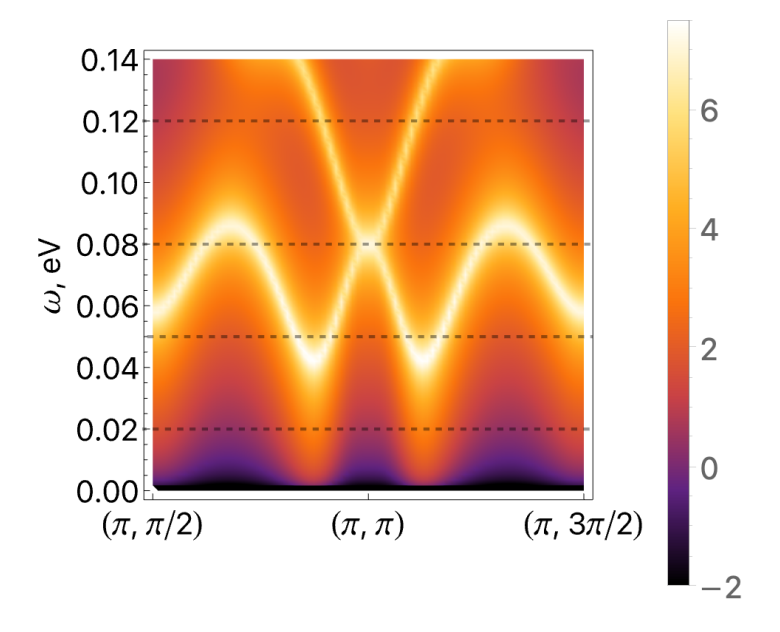


Figure 6: RPA  $\pi$ -flux spin structure factor on a logarithmic scale in the presence of CDW order averaged over the x and y-directions. The triplon branch exhibits a characteristic hourglass-like shape, centered around  $80\,meV$ . Dashed lines represent constant energy cuts along the 2D Brillouin zone in Fig. 7.

peak emerges at  $(\pi, \pi)$  indicating that this energy corresponds to the center of the hourglass dispersion. At higher energies, the central intensity weakens again and the triplon branch forms a complex pattern. It is worthwhile to additionally explore the cut along the  $(\pi, 0)$  direction in the Brillouin zone. The bare spin structure factor shows a strong gap at low energies and broad spinon continuum at higher energies. In contrast, RPA spin structure factor demonstrates an additional peak inside the gap, coming from the triplon branch, while the overall intensity of the spinon continuum is reduced.

Motivated by neutron-scattering experiments in a magnetic field [56], we calculate the spin susceptibility in our model in the presence of a finite magnetic field in Appendix C. We find that the hourglass-like triplon branch splits into two branches, which are shifted in opposite directions by an energy of  $2\Delta E_z$  due to Zeeman coupling. Although experiments require strong magnetic fields to resolve this splitting, such conditions may become possible in the future.

Finally, we comment on an alternative theoretical approach capable of reproducing the hourglass-shaped

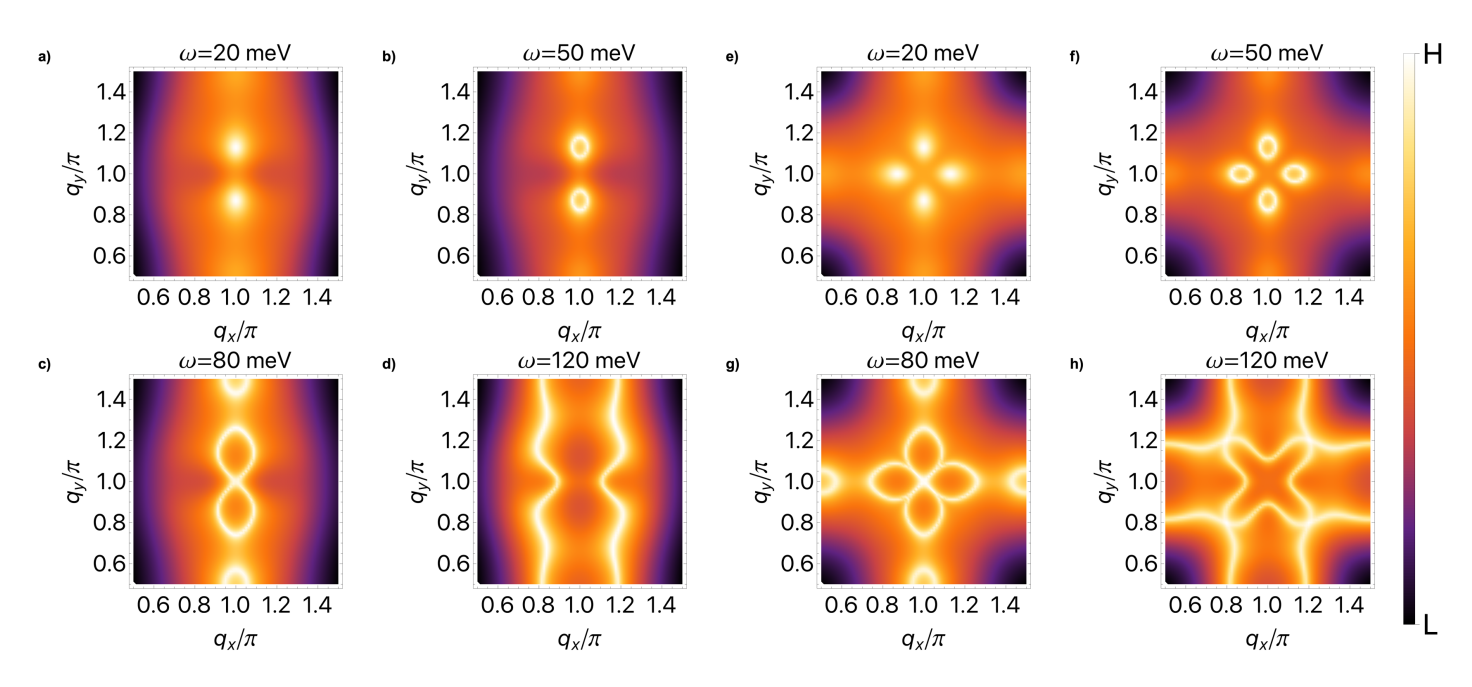


Figure 7: Energy cuts of RPA  $\pi$ -flux spin structure factor in the presence of CDW order. Panels (a)-(d) correspond to energies of 20, 50, 80 and 120 meV (compare to dashed lines in Fig. 6) with the CDW order along the x-direction, while panels (e)-(h) correspond to CDW order averaged over the x and y-directions, and the resulting plots have  $C_4$  symmetry.

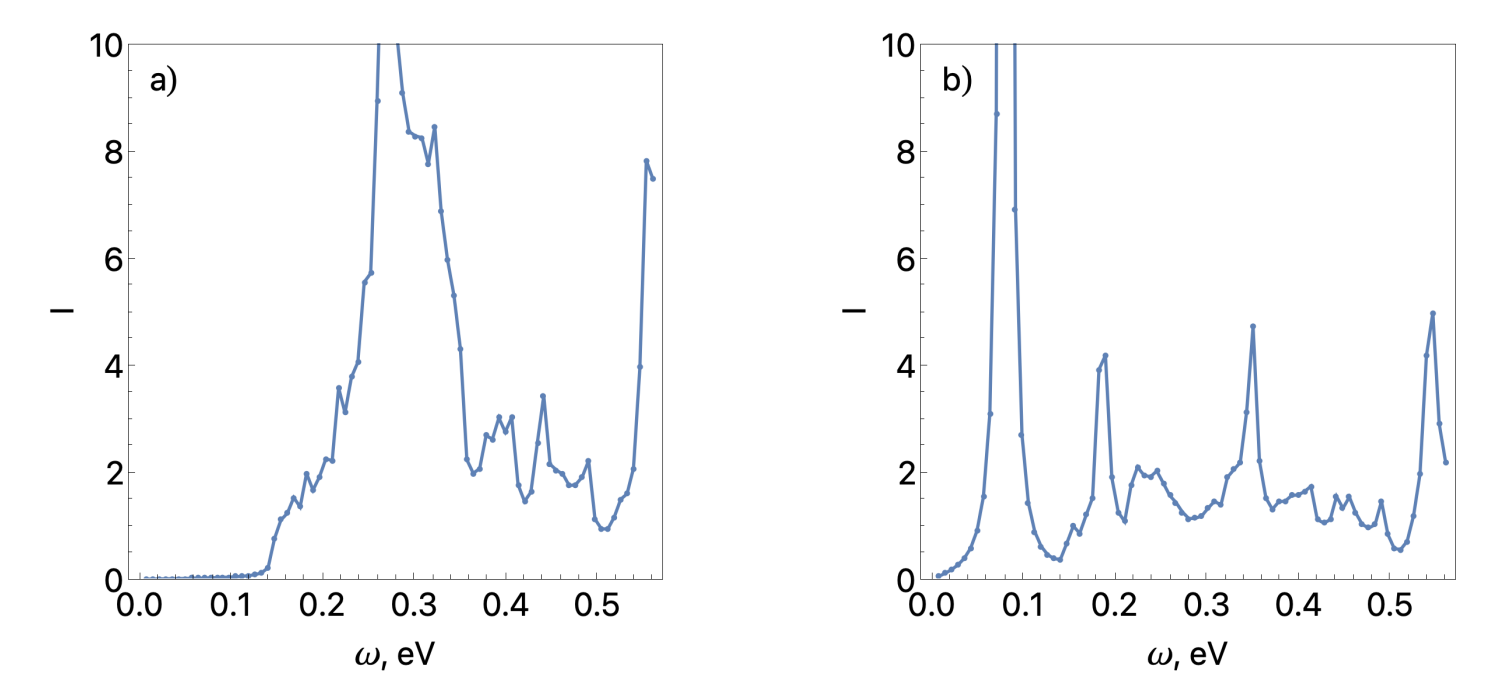


Figure 8: 1D bare (a) and RPA (b)  $\pi$ -flux spin structure factor at fixed momentum  $(q_x, q_y) = (\pi, 0)$  in the presence of CDW order averaged over the x and y directions. Panel (a) shows a spinon continuum starting at  $140 \, meV$ , while panel (b) shows an additional high-intensity triplon branch around  $80 \, meV$  and a redistribution of the spectral weight inside the spinon continuum.

magnetic response, discussed in Appendix D. In particular, we employ the phenomenological theory of coupled spin and charge fluctuations introduced in Ref. [47], to obtain an hourglass-shaped triplon branch outside the spinon continuum. Although this approach is valuable for its simplicity, the RPA-based susceptibility calculated in the main text offers a more direct and microscopic route to reproduce the experimental observations.

#### 4 Conclusions

We have provided a detailed view of the spin structure factor in the ground state of a doped antiferromagnet with period 4 charge density wave order. It is assumed that the intermediate scale spin physics is that of the a particular spin liquid, as is required for consistency with the structure of the intermediate temperature pseudogap. The spinons eventually confine at low energies, by the condensation of a Higgs field, B, which produces the CDW order and simultaneously quenches the emergent gauge field. Near the charge-ordering wavevector, a RPA analysis of the interaction between the spinons produces the 'hourglass' spectrum observed by neutron scattering [33, 34, 35]. Above the hourglass we obtain additional scattering from the spinon continuum which we hope will be studied in subsequent experiments. The spinons are also visible in at other momenta, both in the form of RPA bound states and two-particle continua. This spectrum is a plausible explanation [45] for the high energy scattering observed by RIXS experiments [42, 43, 44], and is present at similar energies. But the detailed form of our high energy spectrum appeares different from current observations e.q. the high intensity scattering disperses downwards from  $(\pi,0)$  to (0,0) in the RIXS observations [43, 42], while that in Fig. 3 disperses upwards. We believe this is a consequence of the rather simple condensed form of the Higgs field, B, in a period 4 CDW state in our computation. It will be of interest to extend our study to the case of fluctuating CDW states using B and SU(2) gauge fields, along the lines of Ref. [11].

We close by summarizing some of the recent arguments for the FL\* state with fermionic spinons in the under-hole-doped cuprates:

- The FL\* theory accounts for the dispersion of the gapped electronic excitations near momentum  $(\pi, 0)$  (the 'antinode'), with the spinons contributing to the broad linewidth [7].
- The existence of the FL\* state allows the possibility of an underlying quantum phase transition to a Fermi liquid (FL) without any symmetry-breaking order parameter [13, 27]. Both FL\* and FL have instabilities to the same d-wave superconductor, and so there is no quantum criticality within the superconducting state. But a strange metal state appears above the superconducting  $T_c$  from FL\*-FL quantum criticality in the presence of random interactions [57]: such a state matches transport [58], thermopower [59], and Hall angle [60] observations.
- The nodal quasiparticles of the low temperature d-wave superconducting state have strongly anisotropic velocities, with  $v_F \gg v_{\Delta}$ , where  $v_F$  is the velocity along the zone diagonal, while  $v_{\Delta}$  is the velocity along the orthogonal direction. This is difficult to understand from a d-wave superconductor descending from a spin liquid with massless Dirac fermion spinons [61, 62, 63, 64], as the spinons have nearly isotropic velocities. However, anisotropic nodal quasiparticles are obtained naturally by confining the FL\* state with such a spin liquid background [65, 9]: the spinons annihilate the Bogoliubov quasiparticles on the 'backsides' of the pockets, and observed Bogoliubov quasiparticles of the d-wave superconductor are those on the 'front side' of the pockets.
- The hole-doped quasiparticles display quantum oscillations at low temperatures and high magnetic fields. These oscillations are associated with *electron* pockets, as indicated by the negative Hall coefficient in this regime. These oscillations are compatible with a model of electron pockets induced by bi-directional charge density wave order [66] only after accounting for the influence of spinons [10].
- The observed structure of the vortex core in the underdoped cuprates is clearly distinct from that of the BCS theory of a d-wave superconductor emerging from a Fermi liquid [67]. The key differences can be described by a theory of the BCS d-wave superconductor emerging from a confinement transition of the FL\* state [68, 11].
- The hole pockets survive in a T=0 FL\* state with a non-zero quasiparticle residue around the hole pocket, even in the presence of the coupling to spinons [7]. Recent work [11] examined thermal fluctuations of a SU(2) gauge theory describing the spinons, at temperatures above a superconducting or charge-ordered ground state (the spinons are confined in these low temperature states). They

showed that such thermal fluctuations do indeed convert the photoemission spectral weight to that of the observed 'Fermi arcs' in the intermediate temperature pseudogap regime.

• Finally, we note the evidence from ADMR and the Yamaji effect [30, 31, 32], which was discussed in Section 1.

#### Acknowledgements

This research was supported by NSF Grant DMR-2245246 and by the Simons Collaboration on Ultra-Quantum Matter which is a grant from the Simons Foundation (651440, S. S.). P.M.B. acknowledges support by the German National Academy of Sciences Leopoldina through Grant No. LPDS 2023-06 and the Gordon and Betty Moore Foundation's EPiQS Initiative Grant GBMF8683. The Flatiron Institute is a division of the Simons Foundation.

#### A Theoretical details

In the basis  $F_{2,q} = (f_{2,q}, f_{2,q+K_x}, f_{2,q+2K_x}, f_{2,q+3K_x})$ , the Hamiltonian in Eq. (9) becomes a  $4 \times 4$  matrix:

$$H_{f_2,f_2} = -t^{f_2} F_{2,q}^{\dagger} \begin{pmatrix} \varepsilon_0(\boldsymbol{q}) & \varepsilon_1(\boldsymbol{q}) & \varepsilon_2(\boldsymbol{q}) & \varepsilon_1^*(\boldsymbol{q} + 3K_x) \\ \varepsilon_1(\boldsymbol{q})^* & \varepsilon_0(\boldsymbol{q} + K_x) & \varepsilon_1(\boldsymbol{q} + K_x) & \varepsilon_2(\boldsymbol{q} + K_x) \\ \varepsilon_2(\boldsymbol{q})^* & \varepsilon_1(\boldsymbol{q} + K_x)^* & \varepsilon_0(\boldsymbol{q} + 2K_x) & \varepsilon_1(\boldsymbol{q} + 2K_x) \\ \varepsilon_1(\boldsymbol{q} + 3K_x) & \varepsilon_2(\boldsymbol{q} + K_x)^* & \varepsilon_1(\boldsymbol{q} + 2K_x)^* & \varepsilon_0(\boldsymbol{q} + 3K_x) \end{pmatrix} F_{2,q},$$
(18)

with the matrix elements:

$$\varepsilon_0(\mathbf{q}) = 2\sin q_x (1 + 2\lambda b^2 \cos 2\theta \cos(K_x/2)) + 4\lambda b^2 \sin q_y, 
\varepsilon_1(\mathbf{q}) = i\lambda b^2 \cos 2\theta (e^{-iq_x - i\phi - iK_x/2} - e^{iq_x - i\phi + iK_x/2}) + 2\lambda b^2 \sin 2\theta \sin q_y e^{i\phi} + 2\lambda b^2 \sin q_y e^{-i\phi}, 
\varepsilon_2(\mathbf{q}) = 2\sin q_y (1 + 2\lambda b^2 \sin 2\theta).$$
(19)

To go to a different basis  $\tilde{F}_{q} = (f_{2,q,\delta_1}, f_{2,q,\delta_2}, f_{2,q,\delta_3}, f_{2,q,\delta_4})$  with  $\delta_i$  being a sublattice site, one can use the unitary transformation:

$$H_{\delta_i\delta_j}(\boldsymbol{q}) = U_{\delta_i n} H_{nm}(\boldsymbol{q}) U_{m\delta_j}^{\dagger}, \qquad U_{ab} = (1/2)e^{iK_x ab}$$
(20)

The Heisenberg coupling is represented by a matrix  $\tilde{J}$ . In the basis  $F_{\mathbf{q}} = (f_{\mathbf{q}}, f_{\mathbf{q}+K_x}, f_{\mathbf{q}+2K_x}, f_{\mathbf{q}+3K_x})$ , it reads

$$\tilde{J} = F_n^*(\mathbf{q}) J_{nm} F_m = J F_q^* \begin{pmatrix}
J_0(\mathbf{q}) & J_1(\mathbf{q}) & J_2(\mathbf{q}) & J_1(\mathbf{q} + 3K_x)^* \\
J_1(\mathbf{q})^* & J_0(\mathbf{q} + K_x) & J_1(\mathbf{q} + K_x) & J_2(\mathbf{q} + K_x) \\
J_2(\mathbf{q})^* & J_1(\mathbf{q} + K_x)^* & J_0(\mathbf{q} + 2K_x) & J_1(\mathbf{q} + 2K_x) \\
J_1(\mathbf{q} + 3K_x) & J_2(\mathbf{q} + K_x)^* & J_1(\mathbf{q} + 2K_x)^* & J_0(\mathbf{q} + 3K_x)
\end{pmatrix} F_{\mathbf{q}},$$
(21)

$$J_{0}(\mathbf{q}) = 2\cos q_{x} \left(1 + 2gb^{2}\cos 2\theta\cos(K_{x}/2)\right) + 2\cos q_{y} (1 + 2gb^{2}\sin 2\theta),$$

$$J_{1}(\mathbf{q}) = gb^{2}\cos 2\theta (e^{-iq_{x}-i\phi-iK_{x}/2} + e^{iq_{x}-i\phi+iK_{x}/2}) + 2gb^{2}\sin 2\theta\cos q_{y}e^{-i\phi} + 2gb^{2}\cos q_{y}e^{i\phi},$$

$$J_{2}(\mathbf{q}) = 4gb^{2}\cos q_{y},$$
(22)

We can also add the second, third, and fourth nearest neighbor coupling to reproduce the hourglass features:  $\tilde{J}_0(\boldsymbol{q}) = J_0(\boldsymbol{q}) + 4J'\cos q_x\cos q_y + 2J''(\cos 2q_x + \cos 2q_y) + 4J'''(\cos 2q_x\cos q_y + \cos q_x\cos 2q_y)$ . To produce Fig. 5, we account for the coupling between the  $\pi$ -flux state and other layers of Ancilla model. The full three-layer Hamiltonian is defined in the basis  $(C_{\boldsymbol{q}}, F_{1,\boldsymbol{q}}, F_{2,\boldsymbol{q}})$ , where each operator corresponds to a certain level. In the presence of CDW order, all operators are defined in the reduced Brillouin zone  $C_{\boldsymbol{q}} = (c_{\boldsymbol{q}}, c_{\boldsymbol{q}+K_x}, c_{\boldsymbol{q}+2K_x}, c_{\boldsymbol{q}+3K_x})$  and similarly for  $F_{1,\boldsymbol{q}}, F_{2,\boldsymbol{q}}$ . The full Hamiltonian consists of three blocks:

 $H_{c,c}(\mathbf{q}) = diag(\epsilon_c(\mathbf{q}), \epsilon_c(\mathbf{q} + K_x), \epsilon_c(\mathbf{q} + 2K_x), \epsilon_c(\mathbf{q} + 3K_x))$  and  $H_{f_1,f_1}$  has the same structure with  $\epsilon_f$  instead of  $\epsilon_c$ . The coupling between the first and second layers is described via a hybridization field  $H_{c,f_1} = \Phi I_{4\times 4}$ . The block  $H_{f_2,f_2}$  corresponds to the Hamiltonian of the  $\pi$ -flux state introduced earlier. The B field is defined according to Eq. (7). For convenience, we redefine the operator  $\tilde{f}_2^{\dagger}(\mathbf{k}) = e^{i\phi_2} f_2^{\dagger}(k_x - K_x/2 + \pi/2, k_y + \pi/2)$  to absorb the prefactor appearing in B. The matrix form of B reads:

$$ig_{e}B = ibg_{e} \begin{pmatrix} S_{1} & S_{2}e^{i\phi} & S_{2} & S_{1}e^{i\phi} \\ S_{1}e^{i\phi} & S_{1} & S_{2}e^{i\phi} & S_{2} \\ S_{2} & S_{1}e^{i\phi} & S_{1} & S_{2}e^{i\phi} \\ S_{2}e^{i\phi} & S_{2} & S_{1}e^{i\phi} & S_{1} \end{pmatrix},$$

$$(23)$$

The Hamiltonian block  $H_{f_2,f_2}$  should also be modified

$$H_{f_2,f_2}(\boldsymbol{q}) = t^{f_2} (F_2)_{\boldsymbol{q}}^* \begin{pmatrix} \varepsilon_0(\boldsymbol{q}) & 0 & \varepsilon_2(\boldsymbol{q}) & 0 \\ 0 & \varepsilon_0(\boldsymbol{q} + K_x) & 0 & \varepsilon_2(\boldsymbol{q} + K_x) \\ \varepsilon_2(\boldsymbol{q})^* & 0 & \varepsilon_0(\boldsymbol{q} + 2K_x) & 0 \\ 0 & \varepsilon_2(\boldsymbol{q} + K_x)^* & 0 & \varepsilon_0(\boldsymbol{q} + 3K_x) \end{pmatrix} (F_2)_{\boldsymbol{q}}, \tag{24}$$

$$\varepsilon_0(\mathbf{q}) = 2\sin(q_x + \pi/4), \quad \varepsilon_2(\mathbf{q}) = 2\sin(q_y + \pi/2).$$
 (25)

After diagonalizing the Hamiltonian, we use Eq. (17) to compute the susceptibility. It can be seen from Eq. (17) that the susceptibility is invariant with respect to going from  $f_2(\mathbf{k})$  to the  $\tilde{f}_2(\mathbf{k})$  basis.

### B RPA $\pi$ -flux

In this Appendix we compute RPA susceptibility of the  $\pi$ -flux state without the CDW order, see Fig. 9. The spectrum remains gapless and Dirac-like spinon continuum near  $(\pi, \pi)$  is still visible. An additional triplon branch emerges at higher energies and merges with the spinon continuum near  $(\pi, \pi)$ . Therefore, including the CDW is crucial in obtaining the hourglass-like spin-structure factor.

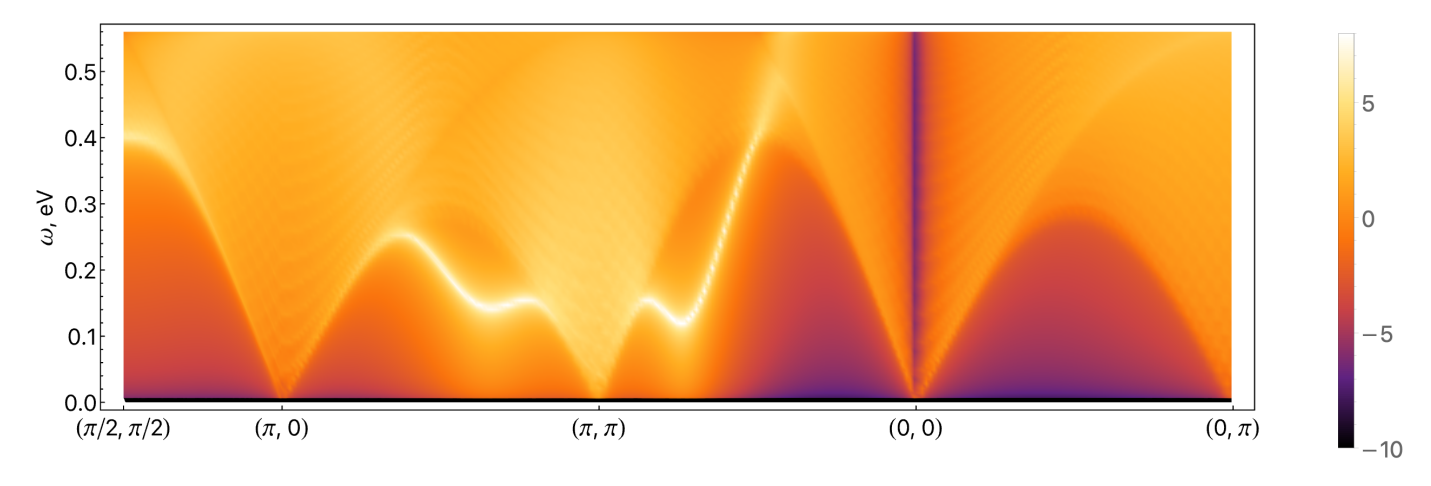


Figure 9: RPA  $\pi$ -flux spin structure factor, shown on a logarithmic scale, without CDW order. The spinon continuum retains a Dirac-like shape near  $(\pi, \pi)$ , while a triplon branch at high energies merges with the spinon continuum near  $(\pi, \pi)$ .

# C Adding magnetic field

In this Appendix we analyze how the spin structure factor changes in the presence of a magnetic field, applied perpendicularly to the sample. The energy bands experience a Zeeman splitting, since the Hamiltonian becomes  $H_B = H_0 + \mu B S^z$ . Spin susceptibilities are defined in the standard way:

$$\chi_{zz}(\omega, q) = \frac{1}{2} \left( \chi_{\uparrow\uparrow}(\omega, q) + \chi_{\downarrow\downarrow}(\omega, q) \right) \qquad \chi_{+-}(\omega, q) = \chi_{\downarrow\uparrow}(\omega, q). \tag{26}$$

The  $\chi_{\uparrow\uparrow}$  component of susceptibility could be written by generalizing Eq. (12):

$$\chi_{\delta_{i},\delta_{j},(\uparrow\uparrow)}^{0}(\omega,\boldsymbol{q}) = \sum_{\alpha,\beta=1,\dots,4} \sum_{\boldsymbol{k}} \frac{n_{F}(E_{\alpha}(\boldsymbol{k}) + \Delta E_{z}) - n_{F}(E_{\beta}(\boldsymbol{k}+\boldsymbol{q}) + \Delta E_{z})}{\omega + i\delta + E_{\alpha}(\boldsymbol{k}) - E_{\beta}(\boldsymbol{k}+\boldsymbol{q})} F_{\delta_{i}}^{\alpha}(\boldsymbol{k}) F_{\delta_{j}}^{\alpha}(\boldsymbol{k})^{*} F_{\delta_{j}}^{\beta}(\boldsymbol{k}+\boldsymbol{q}) F_{\delta_{i}}^{\beta}(\boldsymbol{k}+\boldsymbol{q})^{*},$$
(27)

, where  $\Delta E_z$  is the Zeeman splitting. Since the scattering occurs between the same spin species, shifted by the same energy,  $\chi_{\uparrow\uparrow}$  component of susceptibility is not affected by the magnetic field. The  $\chi_{\uparrow\downarrow}$  component is defined in the following way:

$$\chi_{\delta_{i},\delta_{j},(\uparrow\downarrow)}^{0}(\omega,\boldsymbol{q}) = \sum_{\alpha,\beta=1,\dots,4} \sum_{\boldsymbol{k}} \frac{n_{F}(E_{\alpha}(\boldsymbol{k}) + \Delta E_{z}) - n_{F}(E_{\beta}(\boldsymbol{k}+\boldsymbol{q}) - \Delta E_{z})}{\omega + i\delta + E_{\alpha}(\boldsymbol{k}) - E_{\beta}(\boldsymbol{k}+\boldsymbol{q}) + 2\Delta E_{z}} F_{\delta_{i}}^{\alpha}(\boldsymbol{k}) F_{\delta_{j}}^{\alpha}(\boldsymbol{k})^{*} F_{\delta_{j}}^{\beta}(\boldsymbol{k}+\boldsymbol{q}) F_{\delta_{i}}^{\beta}(\boldsymbol{k}+\boldsymbol{q})^{*}.$$
(28)

The  $\chi_{\uparrow\downarrow}$  component of susceptibility accounts for scattering between opposite spin orientations, therefore, the resulting triplon branch is shifted by  $2\Delta E_z$ . Similarly, the triplon branch coming from  $\chi_{-+}$  component would be shifted by  $2\Delta E_z$  in the opposite direction, as shown in Fig. 10. In practice the splitting is hard to observe since it requires both good energy resolution and strong magnetic fields. However, our prediction could guide future experiments in confirming the triplon spin character of the hourglass-shaped branch.

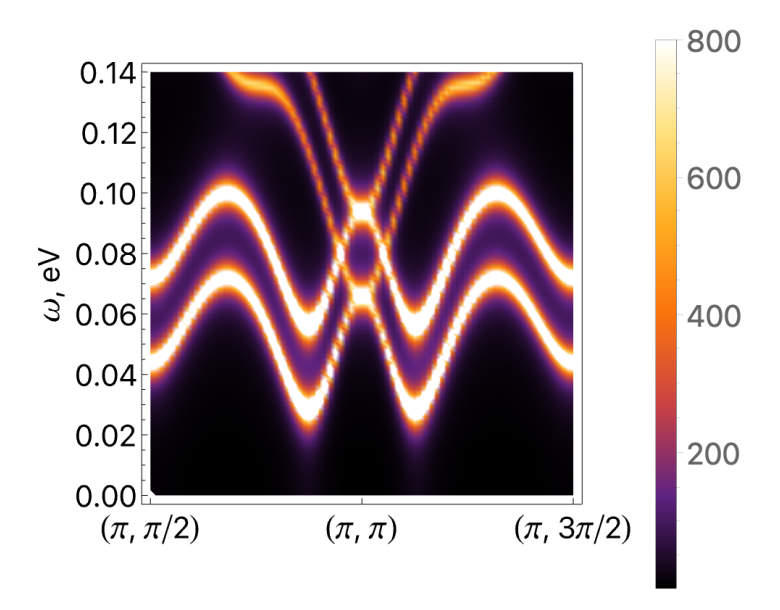


Figure 10: RPA  $\pi$ -flux spin structure factor  $-\Im(\chi_{+-}(\omega,q) + \chi_{-+}(\omega,q))$  in the presence of a magnetic field  $B = 60\,T$  with a Zeeman splitting  $\Delta E_z \approx 0.007\,eV$ . Two triplon branches with  $S_z = \pm 1$  are shifted by  $\pm 2\Delta E_z$  in energy.

## D Alternative approach

In the main part of the paper we obtained the hourglass-like triplon branch as a collective mode of the RPA susceptibility. In this Appendix, we demonstrate that similar features exist in a model of fluctuating stripe charge order, proposed in [47]. We use a phenomenological Lagrangian to describe the coupling between spin and charge fluctuations, which takes the following form:

$$\mathcal{L} = \rho_i \varphi_i^2 + \lambda_2 (\varphi_i \varphi_{i+x} + \varphi_i \varphi_{i+y}) + Q_{b,ij} \varphi_i \varphi_j, \tag{29}$$

where  $\varphi$ -field describes the spin fluctuations and Q-field measures the fluctuations of charge density. Similar to the main text, we choose CDW order with a period of four unit cells:

$$\rho_i = \lambda_1 + 2\lambda_3 \cos\left(\frac{\pi}{2}x + \phi\right), \qquad Q_{b,i-x,i+x} = Q_{b,i-y,i+y} = 2\lambda_4 \cos\left(\frac{\pi}{2}x + 2\phi\right). \tag{30}$$

The phase  $\phi = \pi/4$  ensures that CDW order is bond centered. We define a reduced unit cell operator  $\Phi_q = (\varphi_q, \varphi_{q+\pi/2}, \varphi_{q+\pi}, \varphi_{q+3\pi/2})$ , with the period  $K_x = (\pi/2, 0)$ . In this basis, the Hamiltonian is

$$H(q) = t^{f_2} \Phi_q^* \begin{pmatrix} \varepsilon_0(q) & \varepsilon_1(q) & 0 & \varepsilon_1^*(q+3K_x) \\ \varepsilon_1(q)^* & \varepsilon_0(q+K_x) & \varepsilon_1(q+K_x) & 0 \\ 0 & \varepsilon_1(q+K_x)^* & \varepsilon_0(q+2K_x) & \varepsilon_1(q+2K_x) \\ \varepsilon_1(q+3K_x) & 0 & \varepsilon_1(q+2K_x)^* & \varepsilon_0(q+3K_x) \end{pmatrix} \Phi_q,$$
(31)

where the components of the Hamiltonian are

$$\varepsilon_0(q) = \lambda_1 + \lambda_2(\cos q_x + \cos q_y)$$

$$\varepsilon_1(q) = \lambda_3 e^{-i\phi} + \lambda_4 \left(e^{-i\left(2q_x + \frac{\pi}{2} + \phi\right)} + e^{-i\left(2q_y + \phi\right)}\right).$$
(32)

The eigenenergies satisfy  $\omega^2 \Phi = H(q)\Phi$  and the Green's function of spin fluctuations is:

$$G^{R}(\omega, q)_{0} = ((\omega + i\delta)^{2} - H(q))^{-1}.$$
(33)

We also assume that in the real material there is CDW order in both x and y directions, so for the experimental purposes we compute averaged Green's function  $\bar{G}(\omega, q_x, q_y) = (G(\omega, q_x, q_y) + G(\omega, q_y, q_x))/2$ . The spectral function is defined as  $A_{11}(\omega, q) = \Im \bar{G}_{11}(\omega, q_x, q_y)$ . The  $\pi$ -flux spinons modify the Green's function in the RPA fashion:

$$G^{R}(\omega, q) = ((\omega + i\delta)^{2} - H(q) - g^{2}\chi(\omega, q))^{-1},$$
 (34)

where  $\chi(\omega, q)$  is the  $\pi$ -flux susceptibility in the presence of CDW order, introduced in Eq. (12). Fig. 11 shows the resulting spectral function. We see the hourglass-like dispersion near  $(\pi, \pi)$  coming from the effective Hamiltonian and the spinon continuum at higher energies arising from the RPA corrections.

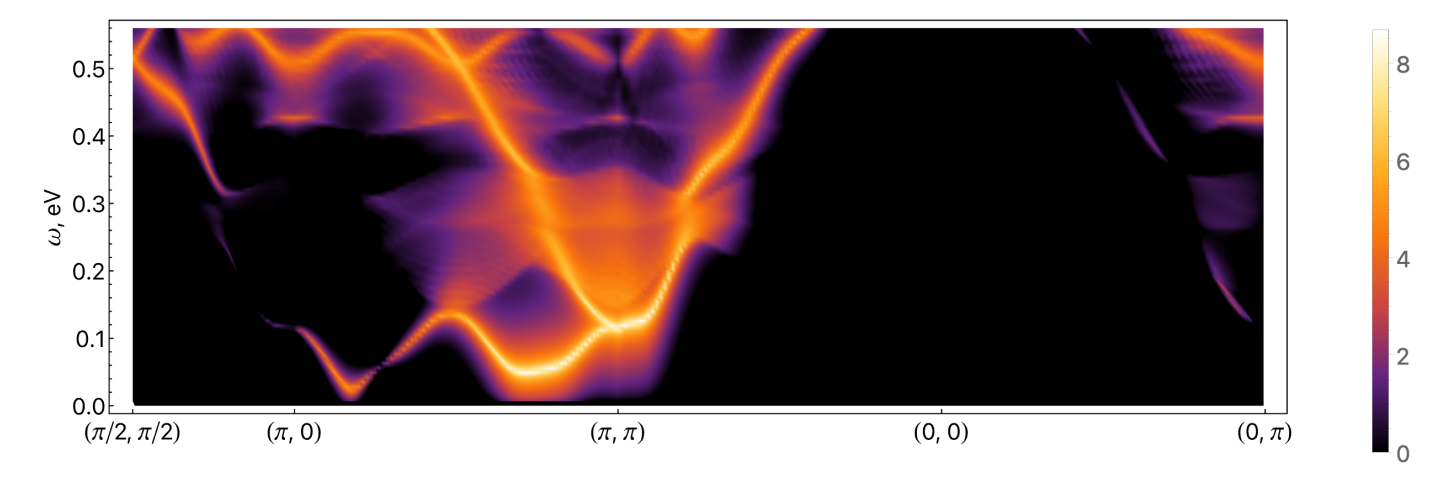


Figure 11: Imaginary part of the retarded Green's function of spin fluctuations, shown on a logarithmic scale. Parameters  $\lambda_1 = 4.15$ ,  $\lambda_2 = 1.54$ ,  $\lambda_3 = 0.07$ ,  $\lambda_4 = 0.66$ . The spectral function demonstrates both a spinon continuum and an hourglass-like triplon branch originating from the spin fluctuations.

### References

[1] N.S. Headings, S.M. Hayden, R. Coldea and T.G. Perring, Anomalous High-Energy Spin Excitations in the High-T<sub>c</sub> Superconductor-Parent Antiferromagnet La<sub>2</sub>CuO<sub>4</sub>, Phys. Rev. Lett. **105** (2010) 247001 [1009.2915].

[2] B. Dalla Piazza, M. Mourigal, N.B. Christensen, G.J. Nilsen, P. Tregenna-Piggott, T.G. Perring, M. Enderle, D.F. McMorrow, D.A. Ivanov and H.M. Rønnow, *Fractional excitations in the square-lattice quantum antiferromagnet*, *Nature Physics* 11 (2015) 62 [1501.01767].

- [3] F. Ferrari and F. Becca, Spectral signatures of fractionalization in the frustrated Heisenberg model on the square lattice, Phys. Rev. B 98 (2018) 100405 [1805.09287].
- [4] N. Ma, G.-Y. Sun, Y.-Z. You, C. Xu, A. Vishwanath, A.W. Sandvik and Z.Y. Meng, Dynamical signature of fractionalization at a deconfined quantum critical point, Phys. Rev. B 98 (2018) 174421 [1803.01180].
- [5] M. Hering, J. Sonnenschein, Y. Iqbal and J. Reuther, Characterization of quantum spin liquids and their spinon band structures via functional renormalization, Phys. Rev. B 99 (2019) 100405
   [1806.05021].
- [6] N.E. Shaik, E. Fogh, B. Dalla Piazza, B. Normand, D.A. Ivanov and H.M. Rønnow, Confined and deconfined spinon excitations in the rectangular-lattice quantum antiferromagnet, Phys. Rev. B 112 (2025) L020410 [2503.14643].
- [7] E. Mascot, A. Nikolaenko, M. Tikhanovskaya, Y.-H. Zhang, D.K. Morr and S. Sachdev, *Electronic spectra with paramagnon fractionalization in the single-band Hubbard model*, *Physical Review B* **105** (2022) 075146 [2111.13703].
- [8] M. Christos, Z.-X. Luo, H. Shackleton, Y.-H. Zhang, M.S. Scheurer and S. Sachdev, A model of d-wave superconductivity, antiferromagnetism, and charge order on the square lattice, Proc. Nat. Acad. Sci. 120 (2023) e2302701120 [2302.07885].
- [9] M. Christos and S. Sachdev, Emergence of nodal Bogoliubov quasiparticles across the transition from the pseudogap metal to the d-wave superconductor, npj Quantum Materials 9 (2024) 4 [2308.03835].
- [10] P.M. Bonetti, M. Christos and S. Sachdev, Quantum oscillations in the hole-doped cuprates and the confinement of spinons, Proceedings of the National Academy of Sciences 121 (2024) e2418633121 [2405.08817].
- [11] H. Pandey, M. Christos, P.M. Bonetti, R. Shanker, S. Sharma and S. Sachdev, Thermal SU(2) lattice gauge theory for the pseudogap and the transition to d-wave superconductivity in the cuprates, arXiv e-prints (2025) arXiv:2507.05336 [2507.05336].
- [12] P.M. Bonetti, M. Christos, A. Nikolaenko, A.A. Patel and S. Sachdev, *Critical quantum liquids and the cuprate high temperature superconductors*, arXiv e-prints (2025) arXiv:2508.20164 [2508.20164].
- [13] T. Senthil, S. Sachdev and M. Vojta, Fractionalized Fermi Liquids, Phys. Rev. Lett. 90 (2003) 216403 [cond-mat/0209144].
- [14] E. Pivovarov and Q. Si, Transitions from small to large Fermi momenta in a one-dimensional Kondo lattice model, Phys. Rev. B 69 (2004) 115104 [cond-mat/0304129].
- [15] T. Senthil, M. Vojta and S. Sachdev, Weak magnetism and non-Fermi liquids near heavy-fermion critical points, Phys. Rev. B 69 (2004) 035111 [cond-mat/0305193].
- [16] A. Paramekanti and A. Vishwanath, Extending Luttinger's theorem to Z₂ fractionalized phases of matter, Phys. Rev. B 70 (2004) 245118 [cond-mat/0406619].
- [17] T. Grover and T. Senthil, Quantum phase transition from an antiferromagnet to a spin liquid in a metal, Phys. Rev. B 81 (2010) 205102 [0910.1277].
- [18] P. Bonderson, M. Cheng, K. Patel and E. Plamadeala, Topological Enrichment of Luttinger's Theorem, arXiv e-prints (2016) [1601.07902].

[19] A.M. Tsvelik, Fractionalized Fermi liquid in a Kondo-Heisenberg model, Phys. Rev. B 94 (2016) 165114 [1604.06417].

- [20] B. Danu, M. Vojta, F.F. Assaad and T. Grover, Kondo Breakdown in a Spin-1/2 Chain of Adatoms on a Dirac Semimetal, Phys. Rev. Lett. 125 (2020) 206602 [2005.10278].
- [21] D.V. Else, R. Thorngren and T. Senthil, Non-Fermi Liquids as Ersatz Fermi Liquids: General Constraints on Compressible Metals, Physical Review X 11 (2021) 021005 [2007.07896].
- [22] A. Panigrahi, A. Tsvelik and P. Coleman, *Breakdown of order fractionalization in the CPT model*, *Phys. Rev. B* **110** (2024) 104520 [2407.08784].
- [23] R.K. Kaul, A. Kolezhuk, M. Levin, S. Sachdev and T. Senthil, *Hole dynamics in an antiferromagnet across a deconfined quantum critical point*, *Phys. Rev. B* **75** (2007) 235122 [cond-mat/0702119].
- [24] R.K. Kaul, Y.B. Kim, S. Sachdev and T. Senthil, Algebraic charge liquids, Nature Physics 4 (2008) 28 [0706.2187].
- [25] Y. Qi and S. Sachdev, Effective theory of Fermi pockets in fluctuating antiferromagnets, Phys. Rev. B 81 (2010) 115129 [0912.0943].
- [26] M. Punk, A. Allais and S. Sachdev, Quantum dimer model for the pseudogap metal, Proceedings of the National Academy of Science 112 (2015) 9552 [1501.00978].
- [27] Y.-H. Zhang and S. Sachdev, From the pseudogap metal to the Fermi liquid using ancilla qubits, Physical Review Research 2 (2020) 023172 [2001.09159].
- [28] J.M. Luttinger, Fermi Surface and Some Simple Equilibrium Properties of a System of Interacting Fermions, Phys. Rev. 119 (1960) 1153.
- [29] M. Oshikawa, Topological Approach to Luttinger's Theorem and the Fermi Surface of a Kondo Lattice, Phys. Rev. Lett. 84 (2000) 3370 [cond-mat/0002392].
- [30] Y. Fang, G. Grissonnanche, A. Legros, S. Verret, F. Laliberté, C. Collignon, A. Ataei, M. Dion, J. Zhou, D. Graf, M.J. Lawler, P.A. Goddard, L. Taillefer and B.J. Ramshaw, Fermi surface transformation at the pseudogap critical point of a cuprate superconductor, Nature Physics 18 (2022) 558 [2004.01725].
- [31] M.K. Chan, K.A. Schreiber, O.E. Ayala-Valenzuela, E.D. Bauer, A. Shekhter and N. Harrison, Observation of the Yamaji effect in a cuprate superconductor, Nature Physics (2025) [2411.10631].
- [32] J.-Y. Zhao, S. Chatterjee, S. Sachdev and Y.-H. Zhang, *Yamaji effect in models of underdoped cuprates*, arXiv e-prints (2025) arXiv:2510.13943 [2510.13943].
- [33] S.M. Hayden, H.A. Mook, P. Dai, T.G. Perring and F. Doğan, The structure of the high-energy spin excitations in a high-transition-temperature superconductor, Nature 429 (2004) 531.
- [34] B. Vignolle, S.M. Hayden, D.F. McMorrow, H.M. Rønnow, B. Lake, C.D. Frost and T.G. Perring, Two energy scales in the spin excitations of the high-temperature superconductor  $La_{2-x}Sr_xCuO_4$ , Nature Physics 3 (2007) 163.
- [35] M.K. Chan, Y. Tang, C.J. Dorow, J. Jeong, L. Mangin-Thro, M.J. Veit, Y. Ge, D.L. Abernathy, Y. Sidis, P. Bourges and M. Greven, Hourglass Dispersion and Resonance of Magnetic Excitations in the Superconducting State of the Single-Layer Cuprate HgBa<sub>2</sub> CuO<sub>4+δ</sub> Near Optimal Doping, Phys. Rev. Lett. 117 (2016) 277002 [1610.01097].
- [36] I. Affleck and J.B. Marston, Large-n limit of the Heisenberg-Hubbard model: Implications for high-T<sub>c</sub> superconductors, Phys. Rev. B **37** (1988) 3774.

[37] I. Affleck, Z. Zou, T. Hsu and P.W. Anderson, SU(2) gauge symmetry of the large-U limit of the Hubbard model, Phys. Rev. B 38 (1988) 745.

- [38] E. Dagotto, E. Fradkin and A. Moreo, SU(2) gauge invariance and order parameters in strongly coupled electronic systems, Phys. Rev. B 38 (1988) 2926.
- [39] N. Read and S. Sachdev, Valence-bond and spin-Peierls ground states of low-dimensional quantum antiferromagnets, Phys. Rev. Lett. 62 (1989) 1694.
- [40] C. Wang, A. Nahum, M.A. Metlitski, C. Xu and T. Senthil, Deconfined quantum critical points: symmetries and dualities, Phys. Rev. X 7 (2017) 031051 [1703.02426].
- [41] Z. Zhou, L. Hu, W. Zhu and Y.-C. He, SO(5) Deconfined Phase Transition under the Fuzzy-Sphere Microscope: Approximate Conformal Symmetry, Pseudo-Criticality, and Operator Spectrum, Physical Review X 14 (2024) 021044 [2306.16435].
- [42] M. Le Tacon, G. Ghiringhelli, J. Chaloupka, M.M. Sala, V. Hinkov, M.W. Haverkort, M. Minola, M. Bakr, K.J. Zhou, S. Blanco-Canosa, C. Monney, Y.T. Song, G.L. Sun, C.T. Lin, G.M. De Luca, M. Salluzzo, G. Khaliullin, T. Schmitt, L. Braicovich and B. Keimer, *Intense paramagnon excitations in a large family of high-temperature superconductors*, *Nature Physics* 7 (2011) 725 [1106.2641].
- [43] H.C. Robarts, M. Barthélemy, K. Kummer, M. García-Fernández, J. Li, A. Nag, A.C. Walters, K.J. Zhou and S.M. Hayden, Anisotropic damping and wave vector dependent susceptibility of the spin fluctuations in La<sub>2-x</sub>Sr<sub>x</sub>CuO<sub>4</sub> studied by resonant inelastic x-ray scattering, Phys. Rev. B 100 (2019) 214510 [1908.03086].
- [44] S. Hameed, Y. Liu, M. Knauft, K.S. Rabinovich, G. Kim, G. Christiani, G. Logvenov, F. Yakhou-Harris, A.V. Boris, B. Keimer and M. Minola, Evolution of spin excitations in superconducting  $La_{2-x}Ca_xCuO_{4-\delta}$  from the underdoped to the heavily overdoped regime, arXiv e-prints (2025) arXiv:2509.06680 [2509.06680].
- [45] S. Sachdev, The foot, the fan, and the cuprate phase diagram: Fermi-volume-changing quantum phase transitions, Physica C 633 (2025) 1354707 [2501.16417].
- [46] M. Vojta and T. Ulbricht, Magnetic Excitations in a Bond-Centered Stripe Phase: Spin Waves Far from the Semiclassical Limit, Phys. Rev. Lett. 93 (2004) 127002 [cond-mat/0402377].
- [47] M. Vojta, T. Vojta and R.K. Kaul, Spin Excitations in Fluctuating Stripe Phases of Doped Cuprate Superconductors, Phys. Rev. Lett. 97 (2006) 097001 [cond-mat/0510448].
- [48] E.C. Andrade and M. Vojta, Disorder, Cluster Spin Glass, and Hourglass Spectra in Striped Magnetic Insulators, Phys. Rev. Lett. 109 (2012) 147201 [1204.6323].
- [49] S.M. Gaw, E.C. Andrade, M. Vojta, C.D. Frost, D.T. Adroja, D. Prabhakaran and A.T. Boothroyd, Hour-glass magnetic spectrum arising from a striped cluster spin-glass ground state in La<sub>1.75</sub>Sr<sub>0.25</sub>CoO<sub>4</sub>, Phys. Rev. B 88 (2013) 165121 [1308.2141].
- [50] Y.-H. Zhang and S. Sachdev, Deconfined criticality and ghost Fermi surfaces at the onset of antiferromagnetism in a metal, Phys. Rev. B 102 (2020) 155124 [2006.01140].
- [51] A. Nikolaenko, J. von Milczewski, D.G. Joshi and S. Sachdev, Spin density wave, Fermi liquid, and fractionalized phases in a theory of antiferromagnetic metals using paramagnons and bosonic spinons, Phys. Rev. B 108 (2023) 045123 [2211.10452].
- [52] R.-H. He, M. Hashimoto, H. Karapetyan, J.D. Koralek, J.P. Hinton, J.P. Testaud, V. Nathan, Y. Yoshida, H. Yao, K. Tanaka, W. Meevasana, R.G. Moore, D.H. Lu, S.K. Mo, M. Ishikado, H. Eisaki, Z. Hussain, T.P. Devereaux, S.A. Kivelson, J. Orenstein, A. Kapitulnik and Z.X. Shen, From a Single-Band Metal to a High-Temperature Superconductor via Two Thermal Phase Transitions, Science 331 (2011) 1579 [1103.2329].

[53] E.A. Ghioldi, M.G. Gonzalez, S.-S. Zhang, Y. Kamiya, L.O. Manuel, A.E. Trumper and C.D. Batista, *Dynamical structure factor of the triangular antiferromagnet: Schwinger boson theory beyond mean field*, *Phys. Rev. B* **98** (2018) 184403 [1802.06878].

- [54] C. Zhang and T. Li, Resonating valence bond theory of anomalous spin dynamics of spin-1/2 triangular lattice Heisenberg antiferromagnet and its application to Ba<sub>3</sub>CoSb<sub>2</sub>O<sub>9</sub>, Phys. Rev. B 102 (2020) 075108 [2003.12688].
- [55] J. Willsher and J. Knolle, Dynamics and stability of U(1) spin liquids beyond mean-field theory: Triangular-lattice  $J_1$ - $J_2$  Heisenberg model, arXiv e-prints (2025) arXiv:2503.13831 [2503.13831].
- [56] R. Coldea, D.A. Tennant, R.A. Cowley, D.F. McMorrow, B. Dorner and Z. Tylczynski, Quasi-1d S = 1/2 antiferromagnet cs<sub>2</sub>cucl<sub>4</sub> in a magnetic field, Phys. Rev. Lett. **79** (1997) 151.
- [57] A.A. Patel, H. Guo, I. Esterlis and S. Sachdev, *Universal theory of strange metals from spatially random interactions*, *Science* **381** (2022) 790 [2203.04990].
- [58] C. Li, D. Valentinis, A.A. Patel, H. Guo, J. Schmalian, S. Sachdev and I. Esterlis, Strange Metal and Superconductor in the Two-Dimensional Yukawa-Sachdev-Ye-Kitaev Model, Phys. Rev. Lett. 133 (2024) 186502 [2406.07608].
- [59] P. Lunts, A.A. Patel and S. Sachdev, Thermopower across Fermi-volume-changing quantum phase transitions without translational symmetry breaking, Phys. Rev. B 111 (2025) 245151 [2412.15330].
- [60] D. Valentinis, J. Schmalian, S. Sachdev and A.A. Patel, Superlinear Hall angle and carrier mobility from non-Boltzmann magnetotransport in the spatially disordered Yukawa-SYK model on a square lattice, to appear (2025).
- [61] F.C. Zhang, C. Gros, T.M. Rice and H. Shiba, A renormalised Hamiltonian approach for a resonant valence bond wavefunction, Superconductor Science and Technology 1 (1988) 36 [cond-mat/0311604].
- [62] G. Kotliar and J. Liu, Superexchange mechanism and d-wave superconductivity, Phys. Rev. B 38 (1988) 5142.
- [63] D.A. Ivanov and T. Senthil, *Projected wave functions for fractionalized phases of quantum spin systems*, *Phys. Rev. B* **66** (2002) 115111 [cond-mat/0204043].
- [64] P.A. Lee, N. Nagaosa and X.-G. Wen, Doping a Mott insulator: Physics of high-temperature superconductivity, Rev. Mod. Phys. 78 (2006) 17 [cond-mat/0410445].
- [65] S. Chatterjee and S. Sachdev, Fractionalized Fermi liquid with bosonic chargons as a candidate for the pseudogap metal, Phys. Rev. B 94 (2016) 205117 [1607.05727].
- [66] N. Harrison and S.E. Sebastian, Protected Nodal Electron Pocket from Multiple-Q Ordering in Underdoped High Temperature Superconductors, Phys. Rev. Lett. 106 (2011) 226402 [1103.4181].
- [67] Y. Wang and A.H. MacDonald, Mixed-state quasiparticle spectrum for d-wave superconductors, Phys. Rev. B 52 (1995) R3876 [cond-mat/9505142].
- [68] J.-X. Zhang and S. Sachdev, Vortex structure in a d-wave superconductor obtained by a confinement transition from the pseudogap metal, Phys. Rev. B 110 (2024) 235120 [2406.12964].